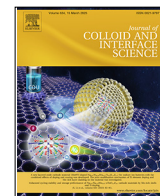




Contents lists available at ScienceDirect

Journal of Colloid and Interface Science

journal homepage: www.elsevier.com/locate/jcis

Microporous metallic scaffolds supported liquid infused icephobic construction



Mengjuan Wu^a, Jie Wang^{b,c}, Sanliang Ling^a, Richard Wheatley^d, Xianghui Hou^{a,*}

^a Faculty of Engineering, University of Nottingham, University Park, Nottingham NG7 2RD, United Kingdom

^b School of Materials Science and Engineering, Nanjing Institute of Technology, Nanjing 211167, China

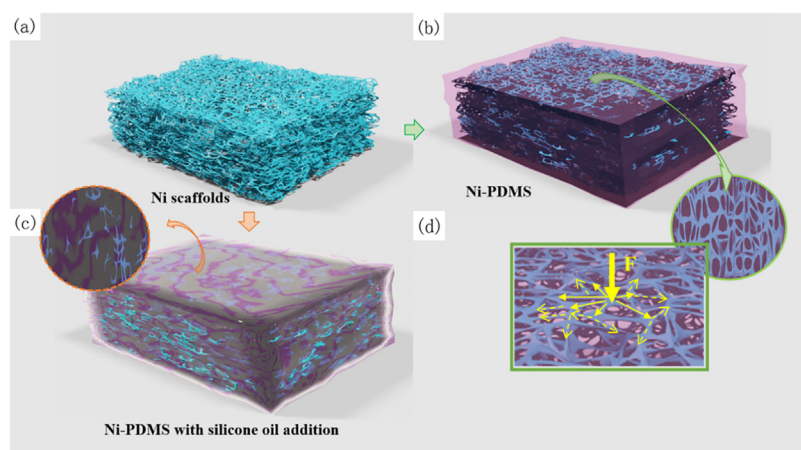
^c Jiangsu Key Laboratory of Advanced Structural Materials and Application Technology, Nanjing 211167, China

^d School of Chemistry, University of Nottingham, University Park, Nottingham NG7 2RD, United Kingdom

HIGHLIGHTS

- A universal approach was proposed to introduce microporous metallic scaffolds in the LIS construction to prompt the potential of LIS for ice mitigation.
- The new LIS construction offered a solution for the rapid oil depletion by restraining the deformation of the matrix material.
- The multiphase icephobic layer structures have demonstrated good icephobicity and significantly improved durability.

GRAPHICAL ABSTRACT



ARTICLE INFO

Article history:

Received 29 September 2022

Revised 30 November 2022

Accepted 7 December 2022

Available online 11 December 2022

Keywords:

Icephobicity
Liquid-infused surfaces
Mechanical durability
Ni scaffolds
Oil infusion

ABSTRACT

Hypothesis: Ice accretion on component surfaces often causes severe impacts or accidents. Liquid-infused surfaces (LIS) have drawn much attention as icephobic materials for ice mitigation in recent years due to their outstanding icephobicity. However, the durability of LIS constructions remains a big challenge, including mechanical vulnerability and rapid depletion of lubricants. The practical applications of LIS materials are significantly restrained, and the full potential of LIS for ice prevention has yet to be demonstrated.

Experiments: A universal approach was proposed to introduce microporous metallic scaffolds in the LIS construction to increase the applicability and durability, and to prompt the potential of LIS for ice mitigation. Microporous Ni scaffolds were chosen to integrate with polydimethylsiloxane modified by silicone oil addition.

Findings: The new LIS construction demonstrated significantly improved durability in icing/de-icing cyclic test, and it also offered a solution for the rapid oil depletion by restraining the deformation of the matrix material. Low ice adhesion strength could be maintained via a micro-crack initiation mechanism. The results indicated that the multi-phase LIS construction consisting of microporous Ni scaffolds

* Corresponding author.

E-mail address: xianghui.hou@outlook.com (X. Hou).

effectively addressed the shackles of the icephobicity deterioration of LIS materials, confirming a new design strategy for the R&D of icephobic surfaces.

© 2022 The Author(s). Published by Elsevier Inc. This is an open access article under the CC BY license (<http://creativecommons.org/licenses/by/4.0/>).

1. Introduction

The adverse icing phenomena such as formation, accretion, and adhesion of ice, snow, or their mixtures could pose serious socio-economic impacts to industries and normal lives and may even, in some cases, lead to severe failures [1,2]. The use of anti-icing surfaces is one of the approaches to effectively alleviate the icing hazards in engineering applications [3–5]. Various icephobic structures have been developed [6,7], which could mainly be categorised into three strategies: 1) To achieve icephobicity by employing superhydrophobic surface [8,9]. The anti-icing performance could be achieved and strengthened with formed air cushions between the micro-nano structures of superhydrophobic surface, which could help with quick slip-away/rebound of the supercooled droplets when they are in contact with the solid surface, thus achieving anti-icing effect. 2) To lower the ice adhesion strength through polymeric elastomer coatings [10,11]. The synergistic effect between the elastomer surfaces with low surface energy decreases the ice adhesion strength, leading to an easy detachment of the accreted ice. 3) To minimise the adhesion strength with slippery liquid-infused porous surfaces (SLIPS) [12,13]. The infused liquid inside the surface micro-cavities could seep out under the control of capillary effect, forming an intact and complete layer coverage and decreasing the ice adhesion strength.

Among these methods, the additions of oil/lubricant in SLIPS have demonstrated great capability of gaining surface icephobicity. Nevertheless, the fast depletion of oil/lubricant from the SLIPS is a great challenge, so the icephobic performance could rapidly deteriorate with the oil depletion. To mitigate this issue, liquid-infused surfaces (LIS) with self-replenishment functions have been prepared for anti-icing and de-icing applications [14,15]. LIS takes the advantage of polymer network to distribute incorporated oil uniformly and to provide a continuous oil supply to the surface. However, the limited mechanical durability of LIS polymer cannot meet the demand for long-term practical applications in ice protection. Wang et al prepared an anti-icing coating using polymers with hydrophilic pendant groups, which could form an aqueous lubricating layer on the as-prepared surfaces [16]. However, the long-term service of LIS could inevitably be limited by the liquidus and soft nature of the infused lubricants, and fast degradation of performance still occurs due to uncontrolled depletion of the lubricants. The icing/de-icing cycles could also result in the loss of the lubricant and even a complete exhaustion [17,18]. After the exhaustion of the infused liquid, the surface rough structure designed for the prevention of the lubricant wrapping effect would undesirably increase the difficulty of de-icing aspect. Currently, LIS constructions are mainly composed of polymeric materials due to their capability of liquid incorporation and distribution, mostly via the expansion of chain networks. However, the oil infusion into the polymer network would significantly weaken the mechanical properties. The decreased mechanical properties, in turn, will also affect the oil maintenance and release under external forces [19,20]. For instance, polydimethylsiloxane (PDMS) with silicone oil addition possesses outstanding icephobic performance, but its surface is easy to be damaged after the excessive oil addition [21].

Overall, the full potential of LIS for ice prevention has yet to be demonstrated, especially for long-term services. There is still lack of effective solutions to mitigate the limited mechanical durability

and rapid oil depletion of LIS structures. To meet the requirements of simultaneous icephobicity and durability for icephobic application, a universal approach is proposed in the present work to introduce microporous metallic scaffolds in the LIS construction. The integration of microporous metallic scaffolds could practically offer a mechanical solution and unfold the potential of LIS. In addition, the difference in elastic modulus between the metallic scaffolds and LIS polymer could lead to different distortions locally which could induce the initiation of micro-cracks at the ice/solid interface under external loads. With the microporous scaffolds, the oil depletion from the LIS construction is also expected to be largely reduced, contributing to the mechanical enhancement. Detailed analysis on sample icephobicity had been carried out from three different aspects including the formation, growth and removal of ice on sample surfaces, which also demonstrated the effectiveness of the new LIS construction.

2. Experimental

2.1. Materials

Microporous nickel (Ni) scaffolds were purchased from TMAX Battery Equipment Ltd (Xiamen, China), with a thickness of 0.3 mm and a porosity of around 85–90%. PDMS Sylgard 184 was purchased from Dow Corning Ltd (California, USA). Silicone oil was supplied by Merck Life Science UK Ltd (Gillingham, UK). Aluminium sheets (Aluminium 2024, Smith Metal Centres Ltd, Biggleswade, UK) with thickness of 0.3 mm were selected as the reference substrates. Laboratory-grade II+ deionised water with a resistivity of 18.2 M Ω ·cm was utilized for the ice block preparation. The testing liquids for surface energy determination included formamide (analytical reagent) and methylene iodide (analytical reagent) were acquired from Fisher Scientific (Loughborough, UK).

2.2. Sample preparation

The Ni scaffolds and Al sheet were both cut into 50 mm \times 20 mm rectangular plates. The plates were first cleaned in an ultrasonic bath with deionized water for 10 min. PDMS Sylgard 184 consisted of a resin (Part A) and a curing agent (Part B). In the first set of experiments, the two parts were mixed together with a weight ratio of 10:1 (A: B) using magnetic stirring to ensure the solution uniformity. Then different amounts of silicone oil (0, 10, 20, 30, 40, 50 wt% with respect to the total solution) were added into the precursor solutions (PDMS-SO), respectively. The solutions were then degassed inside a vacuum oven at room temperature for a duration of 30 min to remove air bubbles. Tab. S1 listed the weight percentages of the added silicone oil in PDMS after curing.

For Ni scaffolds impregnated with PDMS-Silicone oil (Ni/PDMS-SO), the Ni scaffolds were firstly immersed in the prepared PDMS-SO solutions under vacuum (vacuum level: 0.1 bar) for 30 min, to release the air among the microporous structures. The products were then conducted with post-baking treatment in a vacuum oven at 65 °C for 2 h. The vacuum atmosphere could help to remove gases generated during the curing process effectively. The Ni/PDMS-SO samples could be obtained after cooling down. Additional PDMS-SO mixture solutions were applied onto the pre-prepared samples again by a spin coater (KW-4A, Chemat

Group, Northridge, CA, USA) to regulate the surface morphology. For reference samples, the PDMS mixture solution was applied onto Al plates using the spinning coater at a speed of 1000 rpm for 90 s. Same curing treatments were carried out after the spinning process.

Several types of samples were prepared and studied in this work: the sample prepared with Ni scaffolds and pure PDMS filling without silicone oil was named as Ni-PDMS; PDMS with 10, 20, 30, 40, and 50 wt% silicone oil addition were abbreviated as 10SO, 20SO, 30SO, 40SO and 50SO, respectively. Ni scaffolds/PDMS samples with 10, 20, 30, 40, 50 wt% silicone oil addition were designated as NP-10SO, NP-20SO, NP-30SO, NP-40SO and NP-50SO, respectively. For the reference samples, Al alloy substrate was named as Al, while Al substrate/PDMS samples with 10, 20, 30, 40 and 50 wt% silicone oil addition were defined as Al-PDMS, Al-10SO, Al-20SO, Al-30SO, Al-40SO and Al-50SO, respectively.

2.3. Surface characterisation and mechanical tests

Surface morphologies of the as-prepared samples were investigated by an optical microscope (ECLIPSE LV100ND, Nikon) and a scanning electron microscopy (JSM-6490LV, JEOL). Shore hardness tests were conducted with a SAUTER durometer attached with SAUTER test stands TI-AO and TI-D for Shore hardness A and D scales, respectively. The shore hardness A scale was used in this work. 3D surface topography and surface roughness of the samples were measured using a non-contact optical profiler (Zeta-20, KLA-Tencor). For every sample, 10 separate measurements were carried out to calculate the average penetration (Shore) value and minimise the testing error.

Tensile test was carried out using an Instron 5969 Dual Column Tabletop Universal Testing Systems (Instron, High Wycombe, UK) with utilised clamps (Instron 2710–101). The cross-sections of all tested samples were 20 mm × 0.3 mm. The length of the gauge was 6 mm. The applied motion rate was 1.0 mm/min.

2.4. Evaluation of wettability and icephobicity

Water contact angle of the surfaces was measured by a contact angle goniometer (FTA200, First Ten Angstroms, Inc) at room temperature. The static water contact angle was measured with a fixed droplet volume of 5 μL and the pumping out rate was stabilized at 1 μL/s.

Owens-Wendt method was applied to evaluate the surface free energy of the sample surfaces [22]. Three testing liquids included distilled water, formamide and methylene iodide were utilised to determine the surface energy. All of the measurements were conducted under atmospheric conditions at the temperature of 20 °C and the pressure of 1 bar.

Droplet icing tests were performed by observing the icing process of supercooled water droplets on the sample surface in a cold chamber at −20 °C. The volume of the droplet was kept at 4 μL and five different spots on each sample were chosen for comparison. The icing process was recorded to determine the icing behaviours and durations.

Ice growth on the sample surface was investigated by an environmental scanning electron microscopy (Quanta 650 FEG-ESEM, FEI). Water condensation, ice formation and growth were studied under the condition: −10 ~ −2 °C, relative humidity: 90–100%, and pressure: 380 ~ 700 Pa. The ice growth rate was calculated from equation (1) [23]:

$$v = \frac{L}{t} \quad (1)$$

where L is the ice growth length (ice growth direction) (μm), t is the time (s), and v is the ice growth rate (μm/s).

ANSYS software was selected to conduct the comparative 2D plane strain simulation under shear force and gravity on PDMS and Ni-PDMS samples. A combined force including the gravity could be resolved into vertical uniform surface pressure and horizontal shear. An identical force was applied to the two samples.

Ice adhesion strengths were measured using a horizontal shear test system with a pre-prepared ice block (volume: 1.31 mL) attached to the sample surface in an environmental chamber with temperature of −20 °C. For the ice block preparation, a silicone mould was fully filled with 1.31 mL deionised water using pipettor and carefully covered onto the sample surface. Then the samples were kept inside the cold chamber at −20 °C for 3 h, to produce glaze ice block on the samples. The iced area between the mould and the sample was 1.38 cm². The shear test system mainly consisted of a force probe (with diameter of 5 mm), a motion controller, and an ice block attached on tested samples. The schematic set up was shown in Fig. S1. The force probe was used to propel the ice/sample with a velocity of 0.1 mm/min during the test.

With the increase of the shear force, the glaze ice block would overcome the bonding strength and finally detach from the sample surface. The applied force was monitored from the probe, and the ice adhesion strength could be determined using equation (2) [24]:

$$\tau = \frac{F}{A} \quad (2)$$

where τ represents the shear strength (Pa), F refers to the applied force (N), and A is the contact area of the ice block on the sample (m²). Five samples were measured to ensure the data confidence.

Besides, icing/ice detachment cyclic tests were conducted on the samples for 50 times with 3-hour re-freezing intervals. The ice adhesion strength and mass change versus the cyclic tests were also recorded.

3. Results and discussion

3.1. Surface morphologies of NP-SO samples

With the increasing addition of silicone oil, no obvious change occurred on the sample surface, which exhibited smooth and flat throughout the whole modification process, as indicated in Fig. S2 (a) and (b). It could be observed that the surface of the Ni scaffolds was completely covered by the infused PDMS (Fig. 1 (a) and (b)). Fig. 1 (c) and (e) provide the SEM images of the cross-sectional areas of PDMS and NP-40SO, as well as the backscattered electron (BSE) analysis (Fig. 1 (d) and (f)). It was found that the area with light color in BSE images were Ni scaffolds, while the areas with dark color were PDMS. With the increasing oil addition, no obvious change was observed on the sample surfaces, which indicated good compatibility between the Ni scaffolds and the PDMS fillings.

The hardness of as-prepared samples with different oil additions were shown in Fig. 2. The representative values of shore hardness were related to the elastic modulus measured by other methods [25]. In comparison, the pure PDMS exhibited a hardness of 37.6 ± 1.1 (Shore A hardness). While for samples with silicone oil additions, the hardness (Shore A hardness) of NP-10SO, NP-20SO, NP-30SO and NP-40SO were about 33.4 ± 2.1, 29.9 ± 1.2, 24.5 ± 1.2 and 19.8 ± 0.7, respectively. The measured shore hardness showed a steady decreasing trend with increasing silicone oil, which indicated the softening effect of silicone oil infusion. The hardness finally decreased to only 17.1 ± 0.6 (Shore A hardness) for NP-50SO. The reason here could be ascribed to the increased gaps among the macromolecular chains [26], leading to the decrease in cross-link density.

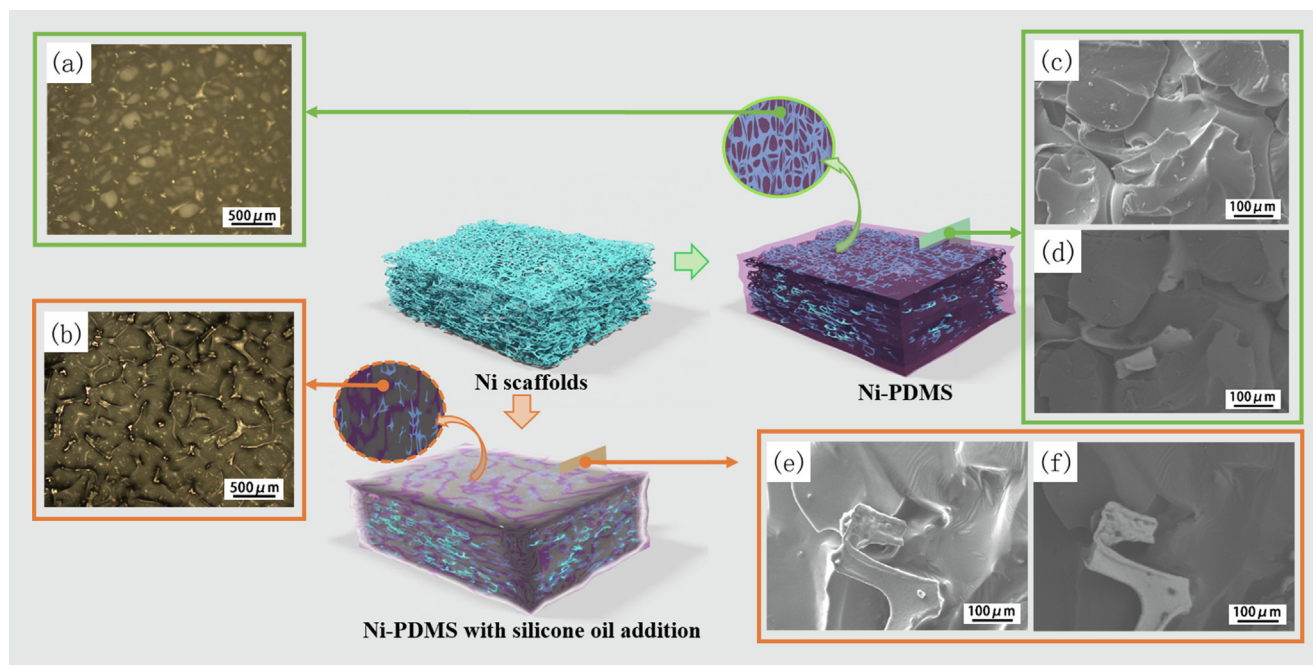


Fig. 1. (a) and (b) Optical microscope images (top view) of Ni-PDMS and NP-40SO; (c) and (e) SEM cross-sectional images of Ni-PDMS and NP-40SO; (d) and (f) BSE images of the cross-sectional areas of Ni-PDMS and NP-40SO.

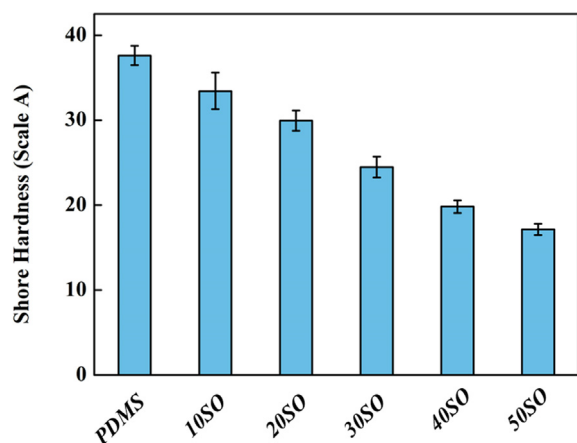


Fig. 2. Shore hardness results of PDMS, 10SO, 20SO, 30SO, 40SO and 50SO samples.

Mechanical performance of the samples was evaluated using tensile test, and the results were provided in [Supplementary Material Fig. S3](#). Significant improved mechanical properties of the LIS construction have been verified with the incorporation of the microporous Ni scaffolds.

3.2. Roughness and wetting behaviours of NP-SO samples

Surface roughness (R_a) of the as-prepared samples has been characterised and compared in [Fig. 3 \(a\)](#). The surface roughness of the as-received Al substrate was $1.40 \pm 0.01 \mu\text{m}$. While for Al-PDMS, with the PDMS layer on top, the measured R_a was $0.75 \pm 0.04 \mu\text{m}$. The as-prepared PDMS layer was smooth and flat, resulting in the decrease of the surface roughness. The average surface roughness of another reference sample Ni-PDMS was about $0.77 \pm 0.07 \mu\text{m}$, very close to that of Al-PDMS. Regarding the NP-SO series samples, only small variations of their surface roughness could be found, ranging from 0.78 to $0.83 \mu\text{m}$. The infused silicone oil would

keep diffusing through the PDMS cross-linked network, forming a lubricated silicone oil overlayer [27]. The thin oil layer could alleviate the small surface undulation caused by the combination of soft polymer and Ni scaffolds, which finally led to the similar surface roughness on different samples.

For the as-prepared NP-SO and the reference samples, water contact angle (WCA) and the contact angle hysteresis (CAH) were measured and shown in [Fig. 3 \(b\)](#). The WCAs of Al plate and Al-PDMS were $101.2 \pm 2.5^\circ$ and $106.1 \pm 0.9^\circ$, respectively. The deviation from the ordinary wettability of pure Al here could be the result of the surface gaseous adsorption derived from the time-dependent wettability [28,29]. For Ni-PDMS, the WCA reached $105.6 \pm 0.6^\circ$, which was also consistent with the inherent wettability of pure PDMS (normally around 104° [30]). For NP-SO series samples, the WCAs showed a steadily increasing trend with higher silicone oil addition. The reason for the WCA increase could be the variation in surface energy. As indicated in [Table 1](#), the surface energy of different samples kept decreasing with the increase of silicone oil. The incorporation of silicone oil also played an important role in lowering the surface energy [31], which finally caused the increased WCAs.

The CAH values also had a clear decreasing trend in [Fig. 3 \(b\)](#). The detailed advancing and receding WCA results were shown in [Supplementary Material Tab. S2](#). With more silicone oil addition, it could be easier for the sample to present slippery behaviours, and CAH of NP-SO samples kept decreasing to lower than 10° . The excess silicone oil could gradually cover the surface, converting a heterogeneous solid-liquid interface to homogeneous liquid-liquid interface and eliminating the ice pinning points, which further led to a reduced liquid-solid contact area [32]. The NP-SO samples exhibited nearly defect-free surfaces, as shown in [Fig. 1](#). The interlocked points at the ice interfaces were reduced, which was favourable to lower the adhesion of the ice layer.

3.3. Anti-icing performance

The icing process of the supercooled water droplets on different samples was illustrated in [Fig. 4 \(a\)](#). It was obvious that the icing

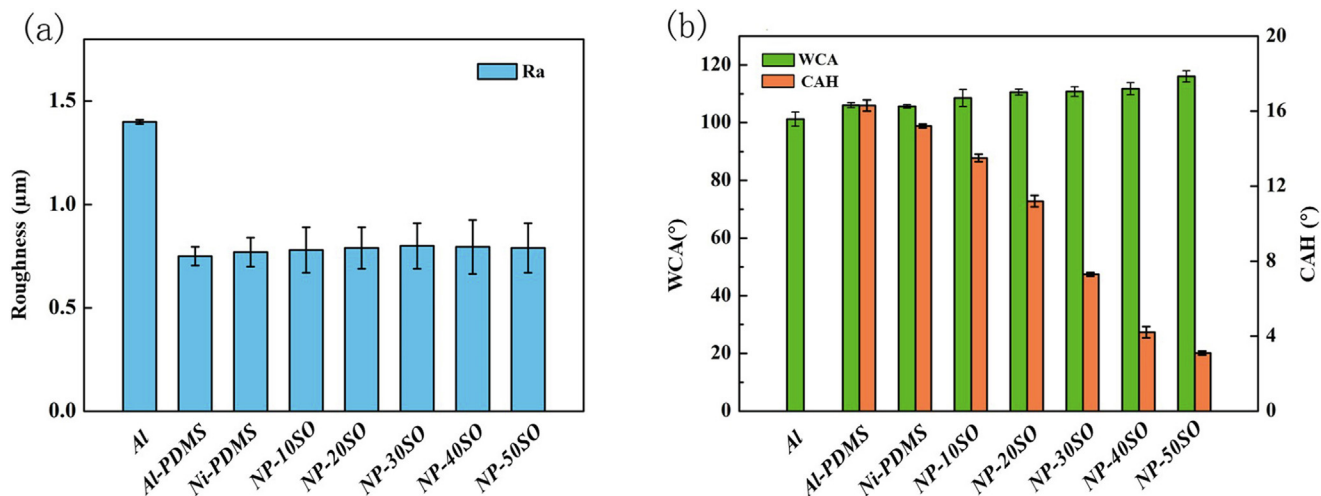


Fig. 3. (a) Surface roughness and (b) Wettability of PDMS, Ni-PDMS and NP-SO series samples.

Table 1
Surface free energy measurement of Al-PDMS, Ni-PDMS and NP-SO series.

Samples	Surface free energy (mJ/m ²)
Al-PDMS	38.22
Ni-PDMS	38.64
NP-10SO	33.96
NP-20SO	33.16
NP-30SO	32.71
NP-40SO	31.84
NP-50SO	29.78

layer always formed from the solid-liquid interface and spread to the top region of the droplet. The ice nucleus was first initiated at the interface, and it then gradually grow into large ice crystals upwards, and finally the whole droplet turned into ice. The water droplet took the shortest time to freeze on Al plate, only 9 s. While for Ni-PDMS, the total icing duration was prolonged to 61 s. As they had the same PDMS top layer, the freezing delay was mainly ascribed to the difference in thermal resistance of the different

samples. Once the sessile droplets (still at room temperature) were dripped onto the sample surfaces, heat exchange took place. The heat would be released along with the ice-solid interfaces, as shown in Fig. 4 (b). The prepared top PDMS layer on Al-PDMS and Ni-PDMS had a similar thickness, bringing no difference to the thermal resistance. While for the bottom layers, it was obvious that the thermal conductivity of the pure Al substrate (237 W/m·K [33]) was much higher than that of Ni/PDMS composite structure (the thermal conductivity of the PDMS filling is only 0.15 W/m·K [34]). So the thermal resistance was much higher than that of Al-PDMS, leading to a longer icing duration.

When water droplets contacted with Ni-PDMS series samples, the icing time on tested surfaces gradually increased with higher silicone oil infusion. The phenomenon could be explained by the increased energy barrier for ice nucleation. The homogenous nucleation contributes the majority of the icing process on ideal lubricated surfaces, while for a normal solid surface such as a metallic substrate, the heterogeneous nucleation process contributes the major part of the icing process [35]. The free energy barriers for homogeneous nucleation (ΔG_{homo}) and heterogeneous

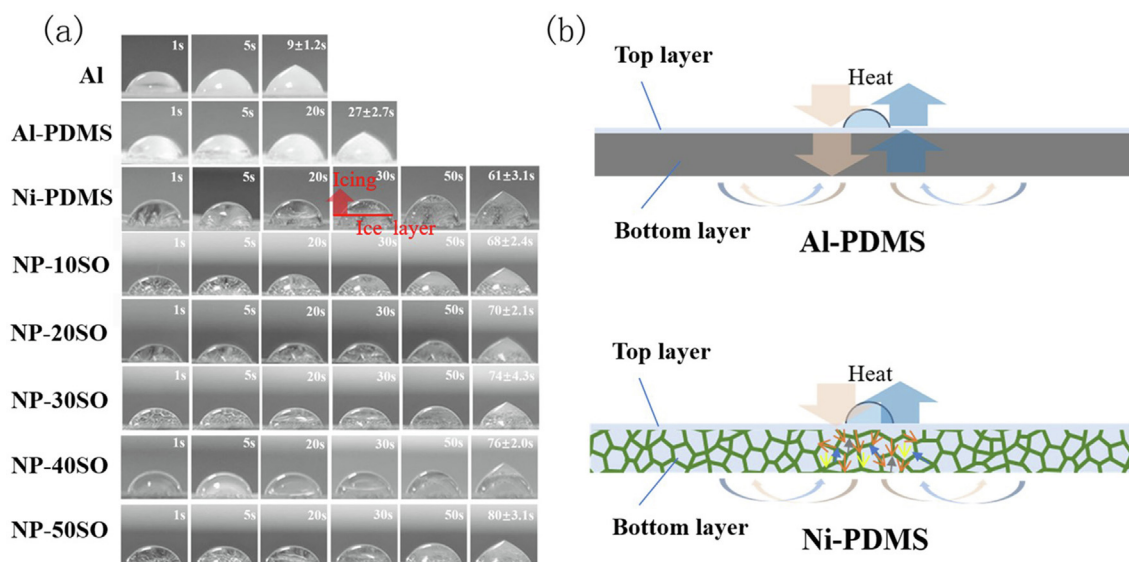


Fig. 4. Icing process of water droplets on different surfaces (a) Al plate, Al-PDMS, Ni-PDMS, NP-SO series under -20 °C. (b) Schematic diagram for thermal conduction of Al-PDMS and Ni-PDMS.

nucleation (ΔG_{hete}) could be estimated using the following equations (3)-(5) [36]:

$$\Delta G_{homo} = -\frac{4}{3}\pi r^3 \Delta G_V + 4\pi r^2 \delta_{IL} \tag{3}$$

$$\Delta G_{hete} = \left(-\frac{4}{3}\pi r^3 \Delta G_V + 4\pi r^2 \delta_{IL}\right) S(\theta) = \Delta G_{homo} S(\theta) \tag{4}$$

$$S(\theta) = \frac{1}{4}(2 + \cos\theta)(1 - \cos\theta)^2 \tag{5}$$

where r means the nucleation radius, ΔG_V shows the driving force during the solidification, and δ_{IL} represents the interfacial energy between the ice nucleus and liquid. θ indicates the contact angle of the nucleus on specific solid surface, which is approximately equal to the measured contact angle of a droplet on a flat surface. The value of $S(\theta)$ is between 0 and 1.

Regarding NP-10SO to NP-50SO, as shown in Fig. 4 (a), the nucleation could be classified as heterogeneous. As the formed surface oil layer would be thickened with the increasing silicone oil addition, ΔG_{hete} on these samples showed an obvious trend, closing to the value on ideal lubricated surfaces (ΔG_{homo}). More energy was

needed for initiating the icing process, resulting in the delayed ice formation.

The results of icing delay indicated that with the microporous Ni scaffolds, the overall thermal resistance of the multiphase layers was increased, which caused the delay of the ice formation. More importantly, the advantage of high energy barrier for ice nucleation on LIS still remained. The good anti-icing performance of LIS had been well retained with the introduction of the microporous Ni scaffolds.

3.4. Water condensation and ice growth

Fig. 5 (a) illustrated the ice growth state near the edge of the Ni-PDMS sample, where the ice grew from left and then spread to the sample surface gradually. It was essential to form solid ice nucleus for the continuous growth of the ice crystals. Ice tended to nucleate on the sample holder at first rather than on the Ni-PDMS surface. The simultaneous evaporation of condensed water droplets would take place along with the ice solidification. The reason for the simultaneous evaporation of the remaining water droplet was the decrease in the environmental humidity inside the chamber

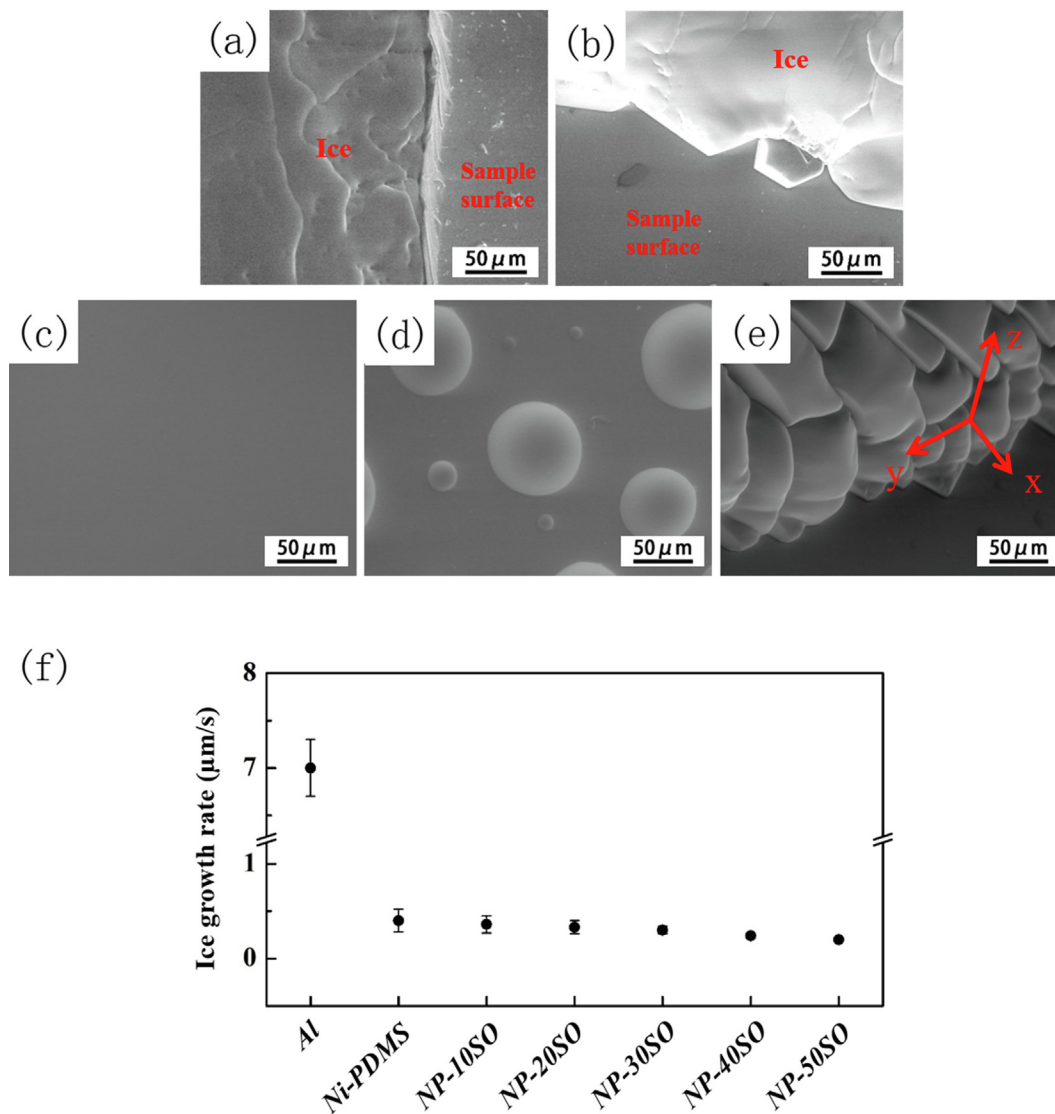


Fig. 5. (a)-(b) ESEM observations on Ni-PDMS: (a) Ice growth near the edge of the sample, (b) Ice growth on the surface; (c)-(e) ESEM images of Ni-40SO sample: (c) As-prepared state, (d) Water condensation, (e) Ice accumulation; (f) Values of ice growth rate on various samples.

(from 99.7% to 90.8%) at the moment of the ice formation, and the water molecules in atmosphere would attach to the formed ice crystal and participate in the ice growth. Meanwhile, due to the exothermic effect of ice formation, the real-time temperature showed a slight increase (from -6.7 °C to -4.2 °C at first, then returned to -6.7 °C). The integrated factors including lowered humidity and increased temperature made the condensed water droplets unable to stay on the Ni-PDMS surface. Fig. 5 (b) showed the ice growth on the Ni-PDMS sample. The formed ice crystal on sample surface was quite large, and only some small ice crystals grew slowly from the boundary and promoted the ice block expansion. Besides, the detailed process of water condensation and ice growth on Al plate and Ni-PDMS using ESEM observation has also been provided in Fig. S4 to Fig. S6 in Supplementary Material as references.

Fig. 5 (c) and (d) showed the surface state of NP-40SO with/without wetting, exhibiting similar water condensation and droplet distribution as Ni-PDMS sample. Fig. 5 (e) showed the ice growth on NP-40SO. Compared with the Ni-PDMS sample, the ice mainly grew in the z direction, leading to the obvious increase in ice thickness on NP-40SO. It was difficult for the ice growth in the x direction, which could be ascribed to the difficulty of ice nucleation at solid-ice interfaces deriving from the fairly high energy barrier. Therefore, the ice growth on existed ice layer was much faster than that on NP-40SO, forming the accumulated ice layer as indicated in Fig. 5 (e).

The surface ice growth rates on the different samples were also depicted in Fig. 5 (f). With respect to the quick ice growth on Al plate, the growth rate of ice had an obvious decrease in NP-SO series. It indicated that the infusion of silicone oil could slow down the ice growth. Also, no negative impact was observed in the icing process on LIS by the introduction of Ni scaffolds. The results further confirmed that NP-SO series samples exhibited strong inhibiting effects on the spread of ice.

3.5. Ice adhesion and evaluation of durability

Fig. 6 (a) showed the ice adhesion strength of different samples. In Fig. 6 (a), the ice adhesion strength of Al plate was maintained at 217.90 ± 6.39 kPa after the icing/de-icing cycles at -20 °C. The measured shear strength decreased to 115.88 ± 8.51 kPa when its surface was covered with PDMS layer. The sample surface was damaged after 28 icing/de-icing cycles. The PDMS top layer was peeled off from the Al plate due to the high ice adhesion strength,

and the surface lose its icephobicity once part of the coating was removed. For Ni-PDMS samples shown in Fig. 6 (a), the addition of microporous Ni scaffold could help to lower the ice adhesion strength to 29.28 ± 2.89 kPa.

Fig. 6 (b) compared the ice adhesion strengths of NP-SO series samples during 50 icing/de-icing cycles at -20 °C. From Ni-PDMS to NP-40SO, the ice adhesion showed a slowly decreasing trend. While for NP-30SO to NP-50SO, the existence of surface oil layer could pose an obvious impact on the ice formation and the ice adhesion strength was lower than 5 kPa.

Fig. 7 (a) showed the variations of oil maintenance ratios in different samples. It was found that the oil mass in the sample nearly remained unchanged during the whole icing/de-icing processes for NP-10SO and NP-20SO. While for NP-30SO and NP-40SO, there was slight decrease of the oil in the two samples. For NP-50SO, an obvious decrease in oil maintenance occurred while the ice adhesion strength kept increasing during the whole process, from 0.085 ± 0.03 kPa (1st cycle) to 7.53 ± 1.89 kPa (50th cycle). The main reason here was that the surface oil layer was much thicker so that it was easier to be depleted than other samples, and there was not enough time for the supplement of the incorporated silicone oil to recover the surface oil coverage. Although the as-prepared NP-50SO showed the lowest value of ice adhesion strength, its de-icing performance experienced significant deterioration after 50 icing/de-icing cycles. It was inferred that NP-40SO possessed the most stable ice adhesion strength. The WCA variations of NP-SO series samples versus 50 icing/de-icing cycles were also compared in Fig. S7. The WCA values on NP-40SO had the lowest change, reflecting a minimal surface damage.

As shown in Fig. 7 (b), the oil depletion of Al-SO series samples was much higher than those of NP-SO series samples. The oil maintenance ratio of Al-40SO was 90.11% after 30 cycles test, while the value of NP-40SO was kept at 99.21% after 50 cycles, the deduction in oil depletion had been clearly confirmed. Therefore, the introduction of microporous scaffolds could also offer an effective solution for the rapid oil depletion by restraining the deformation of the LIS construction.

4. Influence of Ni microporous scaffolds on ice adhesion

To analyse the role of microporous Ni scaffolds in lowering ice adhesion strength, a stress simulation was illustrated in Fig. 8. In the de-icing test, when a shear force was applied to remove the

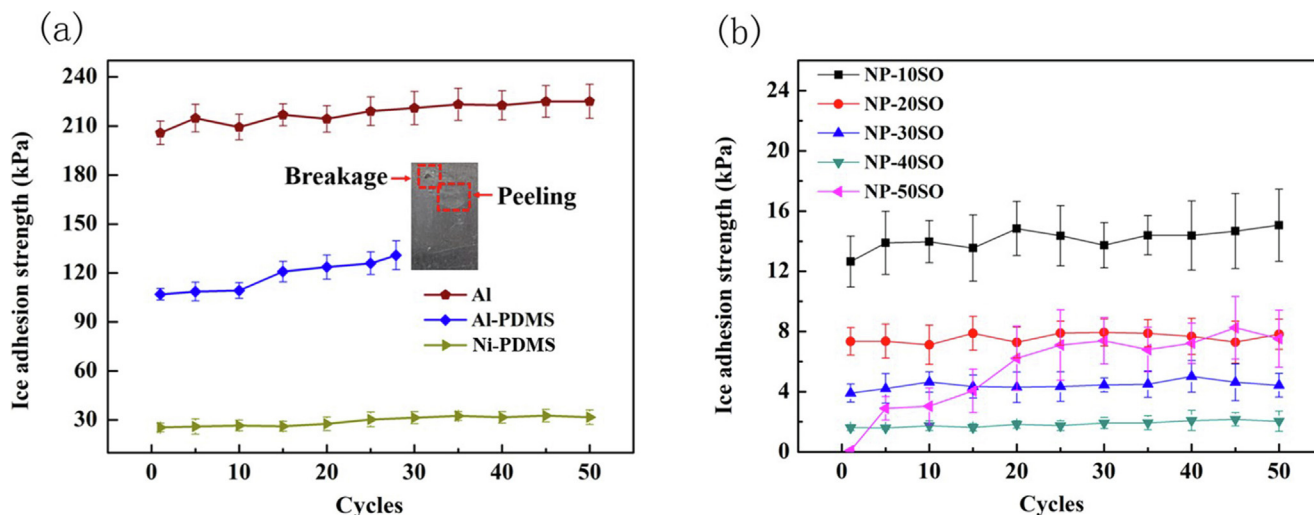


Fig. 6. Ice adhesion strengths of (a) Al, Al-PDMS, and Ni-PDMS and (b) NP-SO series during 50 icing/de-icing cycles.

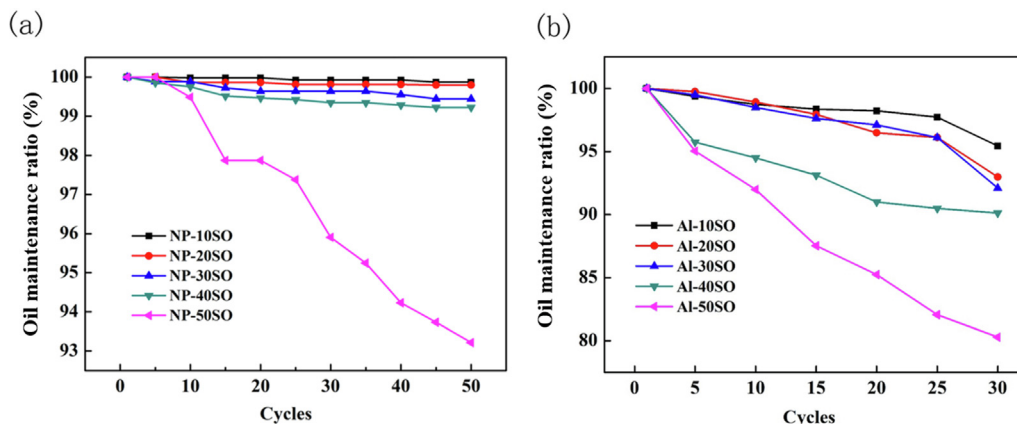


Fig. 7. The oil maintenance ratios in (a) NP-10SO, NP-20SO, NP-30SO, NP-40SO and NP-50SO (b) Al-10SO, Al-20SO, Al-30SO, Al-40SO and Al-50SO.

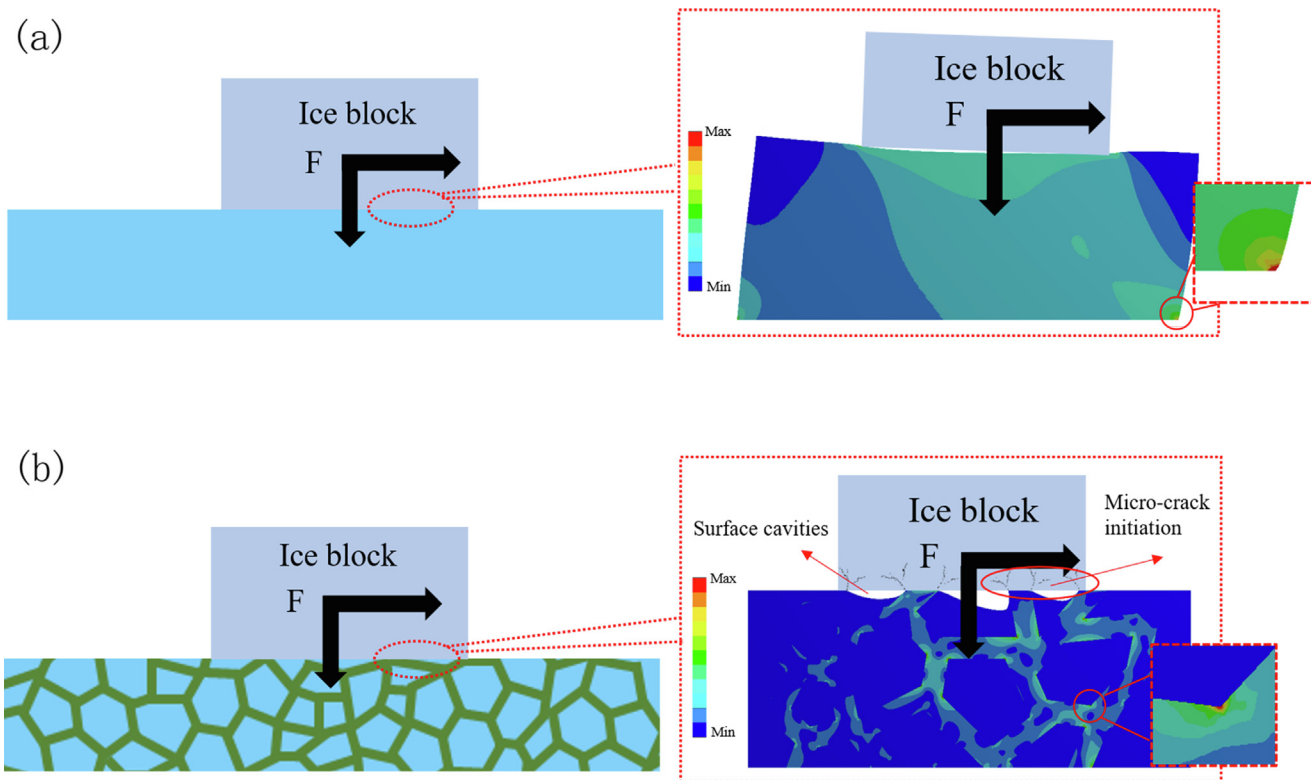


Fig. 8. 2D stress simulation under shear force and gravity on (a) Pure PDMS and (b) Ni-PDMS using ANSYS.

formed ice block from the surface, the combined force including the gravity could be resolved into vertical uniform surface pressure and horizontal shear. For the pure PDMS layer, the maximum stress is mainly located at the bottom right corner area, which introduces large distortion to the PDMS layer. While for Ni-PDMS, the uniformly distributed Ni scaffold carries most of the loading compared with PDMS which is reflected from the colour difference. In the Ni-PDMS structure, the stress in the PDMS matrix would be reduced because the major stress would be carried and re-distributed by the microporous Ni network due to the different elastic modulus between Ni scaffolds and PDMS. This also introduces different distortions at the ice/solid interface areas, generating small surface cavities at the interfaces and leading to the initiation of micro-cracks [37,38]. Compared with the pure PDMS layer, the incorporation of microporous Ni scaffold would significantly improve the mechanical reinforcement effect of the LIS construction and also the de-icing performance.

The reason of the continuous decline in ice adhesion with the increasing SO content in the NP-SO systems could be summarised as follows: 1. With the decreasing hardness of polymeric layer, the elastic mismatch between the polymer and metallic scaffold would increase. It strengthened the stress concentration effect, and the possibility for the initiation of micro-cracks at the solid-ice interface also became higher, causing the easier detachment of ice blocks from the surface [38,39]. 2. Higher oil content would help to maintain a thin oil layer between the ice and solid interface, which was favorable for minimising the ice adhesion strength.

Fig. S8 showed the ice adhesion strength of Al-SO samples during 30 icing/de-icing cycles. With the increase of silicone oil, the measured shear strength of the as-prepared samples decreased from 17.06 ± 1.37 kPa to only 2.58 ± 0.67 kPa (measured in 1st cycle). Nevertheless, the ice adhesion deteriorated with the increased icing/de-icing cycles. Surface damage had been observed on these samples after 30th cycles, which could be attributed to the

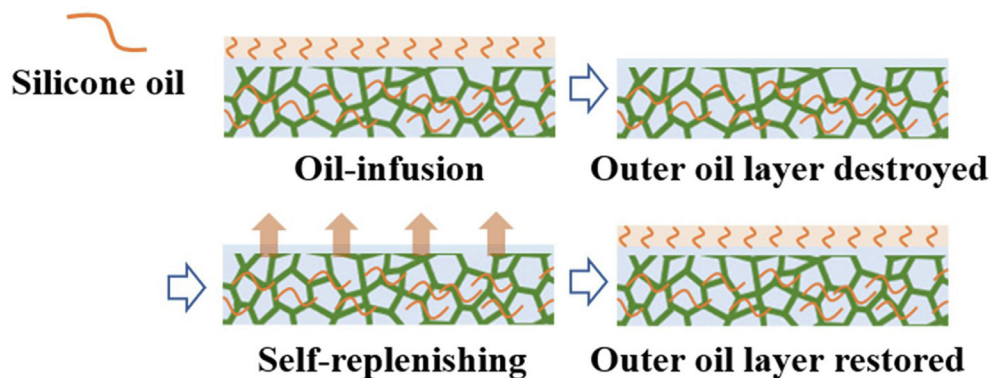


Fig. 9. Schematic diagram explaining the self-replenishment mechanism of the Ni-SO series samples.

oil depletion during the test, leading to the increase of ice adhesion. While comparing the NP-SO and AI-SO samples (shown in Fig. 7), the significantly lowered oil depletion in NP-SO could be ascribed to that the presence of Ni scaffolds restrained the level of deformation of the polymer matrix, which helped to retain the infused oil, since higher deformation could induce increased extrusion of the infused lubricants [40]. The low elastic modulus derived from the LIS enables the infused lubricant with good sensitivity to the shear stress. And the transport of the silicone oil to the surface could easily take place when specific stress was applied onto the LIS. Nevertheless, the introduction of Ni microporous scaffolds into LIS could effectively decrease the overall extent of deformation, slowing down the liquid effusion and depletion, as illustrated in Fig. 8. Besides, the protective frame structures constructed by the microporous scaffolds could also help to minimise the shear-induced loss of infused lubricant and recover to the initial state [41].

Therefore, after 50 cycles, the oil content was maintained at a high level of 99.21% in NP-40SO, as compared with the value of 90.11% in AI-40SO after 30 cycle tests. It is also confirmed the lower ice adhesion had been well maintained with the significantly lowered oil depletion. As shown from the schematics in Fig. 9, the slight loss of oil did not have significant impact on the de-icing performance, because the silicone oil would be replenished from the infused PDMS, reforming oil layer and working as a self-healing system, which also ensured the stability of the de-icing performance [27].

With the introduction of the microporous Ni scaffolds to ensure the mechanical enhancement and to offer additional de-icing mechanisms, the icephobic potential of PDMS-SO have been further demonstrated. The micro-cracks at the solid-ice interface could be readily induced under the shear force, which further weakens the adhesion strength between the formed ice and the surface, prompting the ice detachment from the sample surface. Furthermore, the interconnected network structure formed by microporous metallic scaffold and LIS could work effectively in resisting the external impact energy and minimising the oil depletion. The multiphase structure could also help to distribute the external impact to larger area of the interconnected structure along the metallic scaffold, thus offering effective protection for the LIS construction.

5. Conclusions

In this work, a universal approach was proposed to introduce microporous metallic scaffolds in the LIS construction to increase the applicability and durability, and the potential of LIS was significantly prompted for ice mitigation. Ni scaffolds and PDMS modified silicone oil (NP-SO) system were chosen for the LIS

construction, and the multiphase icephobic layer structures have demonstrated good icephobicity and significantly improved durability. In comparison with recent reports [27,40,42–47] indicated in Tab. S3 (Supplementary Material), the proposed LIS construction in this work demonstrated an obvious advantage in the de-icing aspects. The ice adhesion strength of Ni scaffolds combined with PDMS modified by 40 % silicone oil addition was below 2 kPa and the low ice adhesion strength was maintained even after 50 icing/de-icing cycles. A good level of lubricating effect would be well retained with minimal oil depletion for the enhanced LIS construction. The introduction of microporous Ni scaffolds could help to redistribute the stress during de-icing process, which effectively protected the LIS materials from external load and impact. The multiphase LIS construction could further boost the initiation of micro-cracks at the solid-ice interfaces and prompt an easy ice detachment. Additionally, with the microporous scaffolds, the oil depletion from the LIS construction has also been largely reduced, contributing to the durability enhancement.

The newly developed strategy could effectively alleviate the problem of serious oil depletion and fragility of LIS surfaces by combining the advantage of mechanical durability enhancement and effectiveness in icephobicity. The LIS construction design could also be used in the combinations with diverse polymeric substrates, which further opens the potential in ice protection. For example, the NP-SO system in this work could be developed as gummed tape and attached onto certain engineering surfaces directly like aircraft wings or wind turbines [48]. The good icephobicity, durability and eco-friendly behavior of the new design strategy are likely to prompt the potential of LIS for a wide range of applications.

Author Contributions

Mengjuan Wu: Conceptualization, Data curation, Formal analysis, Investigation, Methodology, Software, Validation, Writing - original draft, Writing - review & editing. **Jie Wang:** Conceptualization, Data curation, Formal analysis, Methodology Validation, Writing - review & editing. **Sanliang Ling:** Resources, Supervision, Validation, Writing - review & editing. **Richard Wheatley:** Resources, Supervision, Validation, Writing - review & editing. **Xianghui Hou:** Conceptualization, Data curation, Funding acquisition, Methodology, Project administration, Resources, Supervision, Validation, Writing - original draft, Writing - review & editing.

Data availability

Data will be made available on request.

Declaration of Competing Interest

The authors declare that they have no known competing financial interests or personal relationships that could have appeared to influence the work reported in this paper.

Acknowledgments

The work is financially supported by the UK Engineering and Physical Sciences Research Council (EPSRC) grants EP/L022494/1, the University of Nottingham Propulsion Futures Beacon for funding under Grant PF016 and PF020 and Scientific Research Foundation of Nanjing Institute of Technology (YKJ202106). The authors acknowledge the use of facilities at Nanoscale and Microscale Research Centre of the University of Nottingham. The joint Ph.D. studentship between the China Scholarship Council (CSC) and The University of Nottingham is also acknowledged.

Appendix A. Supplementary data

Supplementary data to this article can be found online at <https://doi.org/10.1016/j.jcis.2022.12.034>.

References

- [1] K. Golovin, A. Dhyani, M. Thouless, A. Tuteja, Low-interfacial toughness materials for effective large-scale deicing, *Science* 364 (6438) (2019) 371–375.
- [2] F. Zhang, Z. Huang, H. Yao, W. Zhai, T. Gao, Icing severity forecast algorithm under both subjective and objective parameters uncertainties, *Atmos. Environ.* 128 (2016) 263–267.
- [3] P. Wang, Z. Li, Q. Xie, W. Duan, X. Zhang, H. Han, A passive anti-icing strategy based on a superhydrophobic mesh with extremely low ice adhesion strength, *J. Bionic Eng.* 18 (1) (2021) 55–64.
- [4] T. Wu, W.-H. Xu, K. Guo, H. Xie, J.-P. Qu, Efficient fabrication of lightweight polyethylene foam with robust and durable superhydrophobicity for self-cleaning and anti-icing applications, *Chem. Eng. J.* 407 (2021) 127100.
- [5] Y. Qing, C. Long, K. An, C. Hu, C. Liu, Sandpaper as template for a robust superhydrophobic surface with self-cleaning and anti-snow/icing performances, *J. Colloid Interface Sci.* 548 (2019) 224–232.
- [6] S. Gao, B. Liu, J. Peng, K. Zhu, Y. Zhao, X. Li, X. Yuan, Icephobic durability of branched PDMS slippage coatings co-cross-linked by functionalized POSS, *ACS Appl. Mater. Interfaces* 11 (4) (2019) 4654–4666.
- [7] J. Wang, M. Wu, J. Liu, F. Xu, T. Hussain, C. Scotchford, X. Hou, Metallic skeleton promoted two-phase durable icephobic layers, *J. Colloid Interface Sci.* 587 (2021) 47–55.
- [8] G. Wang, Y. Shen, J. Tao, X. Luo, M. Jin, Y. Xie, Z. Li, S. Guo, Facilely constructing micro-nanostructure superhydrophobic aluminum surface with robust icephobicity and corrosion resistance, *Surf. Coat. Technol.* 329 (2017) 224–231.
- [9] X. Wu, F. Yang, G. Lu, X. Zhao, Z. Chen, S. Qian, A breathable and environmentally friendly superhydrophobic coating for anti-condensation applications, *Chem. Eng. J.* 412 (2021) 128725.
- [10] Y. Shen, K. Li, H. Chen, Z. Wu, Z. Wang, Superhydrophobic F-SiO₂/PDMS composite coatings prepared by a two-step spraying method for the interface erosion mechanism and anti-corrosive applications, *Chem. Eng. J.* 413 (2021) 127455.
- [11] X. Shi, X. Lv, J. Lu, Y. Xu, W. Yuan, Y. He, Anti-icing polyimide thin film with microcolumns fabricated by RIE with cooling and PCVD, *Micro & Nano Letters* 17 (1) (2022) 1–8.
- [12] L. Xiao, J. Li, S. Mieszkin, A. Di Fino, A.S. Clare, M.E. Callow, J.A. Callow, M. Grunze, A. Rosenhahn, P.A. Levkin, Slippery liquid-infused porous surfaces showing marine antibiofouling properties, *ACS Appl. Mater. Interfaces* 5 (20) (2013) 10074–10080.
- [13] T.-S. Wong, S.H. Kang, S.K. Tang, E.J. Smythe, B.D. Hatton, A. Grinthal, J. Aizenberg, Bioinspired self-repairing slippery surfaces with pressure-stable omniphobicity, *Nature* 477 (7365) (2011) 443–447.
- [14] G. Chen, S. Liu, Z. Sun, S. Wen, T. Feng, Z. Yue, Intrinsic self-healing organogels based on dynamic polymer network with self-regulated secretion of liquid for anti-icing, *Prog. Org. Coat.* 144 (2020) 105641.
- [15] M. Carloti, I. Cesini, V. Mattoli, A Simple Approach for Flexible and Stretchable Anti-icing Lubricant-Infused Tape, *ACS Appl. Mater. Interfaces* 13 (37) (2021) 45105–45115.
- [16] R. Dou, J. Chen, Y. Zhang, X. Wang, D. Cui, Y. Song, L. Jiang, J. Wang, Anti-icing coating with an aqueous lubricating layer, *ACS Appl. Mater. Interfaces* 6 (10) (2014) 6998–7003.
- [17] X. Tan, Y. Wang, Z. Huang, S. Sabin, T. Xiao, L. Jiang, X. Chen, Facile Fabrication of a Mechanical, Chemical, Thermal, and Long-Term Outdoor Durable Fluorine-Free Superhydrophobic Coating, *Adv. Mater. Interfaces* 8 (11) (2021) 2002209.
- [18] M.J. Kreder, J. Alvarenga, P. Kim, J. Aizenberg, Design of anti-icing surfaces: smooth, textured or slippery?, *Nat. Rev. Mater.* 1 (1) (2016) 1–15.
- [19] Q. Rao, Y. Lu, L. Song, Y. Hou, X. Zhan, Q. Zhang, Highly efficient self-repairing slippery liquid-infused surface with promising anti-icing and anti-fouling performance, *ACS Appl. Mater. Interfaces* 13 (33) (2021) 40032–40041.
- [20] J.S. Wexler, A. Grosskopf, M. Chow, Y. Fan, I. Jacobi, H.A. Stone, Robust liquid-infused surfaces through patterned wettability, *Soft Matter* 11 (25) (2015) 5023–5029.
- [21] J. Zhang, B. Liu, Y. Tian, F. Wang, Q. Chen, F. Zhang, H. Qian, L. Ma, Facile One-Step Method to Fabricate a Slippery Lubricant-Infused Surface (LIS) with Self-Replenishment Properties for Anti-Icing Applications, *Coatings* 10 (2) (2020) 119.
- [22] L. Mazzola, Aeronautical livery coating with icephobic property, *Surf. Eng.* 32 (10) (2016) 733–744.
- [23] M.F. Butler, Instability formation and directional dendritic growth of ice studied by optical interferometry, *Cryst. Growth Des.* 1 (3) (2001) 213–223.
- [24] C. Laforte, C. Blackburn, J. Perron, R. Aubert, Icephobic coating evaluation for aerospace application, 55th AIAA/ASME/ASCE/AHS/SC Structures, Structural Dynamics, and Materials Conference (2014) 1327.
- [25] I.M. Meththananda, S. Parker, M.P. Patel, M. Braden, The relationship between Shore hardness of elastomeric dental materials and Young's modulus, *Dent. Mater.* 25 (8) (2009) 956–959.
- [26] J.H. Kim, M.J. Kim, B. Lee, J.M. Chun, V. Patil, Y.-S. Kim, Durable ice-lubricating surfaces based on polydimethylsiloxane embedded silicone oil infused silica aerogel, *Appl. Surf. Sci.* 512 (2020) 145728.
- [27] K. Xing, Z. Li, Z. Wang, S. Qian, J. Feng, C. Gu, J. Tu, Slippery coatings with mechanical robustness and self-replenishing properties as potential application on magnesium alloys, *Chem. Eng. J.* 418 (2021) 129079.
- [28] J. Wang, H. Memon, J. Liu, G. Yang, F. Xu, T. Hussain, C. Scotchford, X. Hou, Effect of surface adsorption on icing behaviour of metallic coating, *Surf. Coat. Technol.* 380 (2019) 125068.
- [29] J. Wang, J. Liu, N. Neate, M. Bai, F. Xu, T. Hussain, C. Scotchford, X. Hou, Investigation on time-dependent wetting behavior of Ni-Cu-P ternary coating, *J. Alloy. Compd.* 765 (2018) 221–228.
- [30] E. Gee, G. Liu, H. Hu, J. Wang, Effect of varying chain length and content of poly (dimethylsiloxane) on dynamic dewetting performance of NP-GLIDE polyurethane coatings, *Langmuir* 34 (34) (2018) 10102–10113.
- [31] T. Svitova, O. Theodoly, S. Cristiano, R. Hill, C. Radke, Wetting behavior of silicone oils on solid substrates immersed in aqueous electrolyte solutions, *Langmuir* 18 (18) (2002) 6821–6829.
- [32] S. Heydari, R. Jafari, G. Momen, Recent progress in the anti-icing performance of slippery liquid-infused surfaces, *Prog. Org. Coat.* 151 (2021) 106096.
- [33] R. Brandt, G. Neuer, Electrical resistivity and thermal conductivity of pure aluminum and aluminum alloys up to and above the melting temperature, *Int. J. Thermophys.* 28 (5) (2007) 1429–1446.
- [34] J. Mark, *Polymer Data Handbook* Oxford Univ. Press, New York, NY, 1999, p. 363.
- [35] Q. Liu, Y. Yang, M. Huang, Y. Zhou, Y. Liu, X. Liang, Durability of a lubricant-infused Electro-spray Silicon Rubber surface as an anti-icing coating, *Appl. Surf. Sci.* 346 (2015) 68–76.
- [36] C. Wei, B. Jin, Q. Zhang, X. Zhan, F. Chen, Anti-icing performance of super-wetting surfaces from icing-resistance to ice-phobic aspects: Robust hydrophobic or slippery surfaces, *J. Alloy. Compd.* 765 (2018) 721–730.
- [37] Z. He, Y. Zhuo, F. Wang, J. He, Z. Zhang, Design and preparation of icephobic PDMS-based coatings by introducing an aqueous lubricating layer and macro-crack initiators at the ice-substrate interface, *Prog. Org. Coat.* 147 (2020) 105737.
- [38] P. Irajizad, A. Al-Bayati, B. Esлами, T. Shafquat, M. Nazari, P. Jafari, V. Kashyap, A. Masoudi, D. Araya, H. Ghasemi, Stress-localized durable icephobic surfaces, *Mater. Horiz.* 6 (4) (2019) 758–766.
- [39] Z. He, S. Xiao, H. Gao, J. He, Z. Zhang, Multiscale crack initiator promoted super-low ice adhesion surfaces, *Soft Matter* 13 (37) (2017) 6562–6568.
- [40] H. Qian, B. Liu, D. Wu, W. Liu, T. Chowwanonthapunya, D. Zhang, Facile fabrication of slippery lubricant-infused porous surface with pressure responsive property for anti-icing application, *Colloids Surf A Physicochem Eng Asp* 618 (2021) 126457.
- [41] H.N. Kim, S.J. Kim, W. Choi, H.J. Sung, S.J. Lee, Depletion of lubricant impregnated in a cavity of lubricant-infused surface, *Phys. Fluids* 33 (2) (2021) 022005.
- [42] J. Zhang, B. Liu, Y. Tian, F. Wang, L. Ma, Facile One-Step Method to Fabricate a Slippery Lubricant-Infused Surface (LIS) with Self-Replenishment Properties for Anti-Icing Applications, *Coatings* 10 (2) (2020) 119.
- [43] R. Khammas, H. Koivuluoto, Durable Icephobic Slippery Liquid-Infused Porous Surfaces (SLIPS) Using Flame- and Cold-Spraying, *Sustainability* 14 (14) (2022) 8422.
- [44] S. Barthwal, B. Lee, S.H. Lim, Fabrication of robust and durable slippery anti-icing coating on textured superhydrophobic aluminum surfaces with infused silicone oil, *Appl. Surf. Sci.* 496 (2019) 143677.
- [45] L.B. Boinovich, K.A. Emelyanenko, A.M. Emelyanenko, Superhydrophobic versus SLIPS: Temperature dependence and the stability of ice adhesion strength, *J. Colloid Interface Sci.* 606 (2022) 556–566.
- [46] Z. He, C. Wu, M. Hua, S. Wu, D. Wu, X. Zhu, J. Wang, X. He, Bioinspired Multifunctional Anti-icing Hydrogel, *Matter* 2 (3) (2020) 723–734.
- [47] T. Li, Y. Zhuo, V. Håkonsen, J. He, Z. Zhang, Durable low ice adhesion foams modulated by submicrometer pores, *Ind. Eng. Chem. Res.* 58 (38) (2019) 17776–17783.
- [48] L. Wang, M. Wen, M. Zhang, L. Jiang, Y. Zheng, Ice-phobic gummed tape with nano-cones on microspheres, *J. Mater. Chem. A* 2 (10) (2014) 3312–3316.